

## Article

# Biomagnetic Fluid Flow and Heat Transfer Study of Blood with Gold Nanoparticles over a Stretching Sheet in the Presence of Magnetic Dipole

Jahangir Alam <sup>1</sup>, Ghulam Murtaza <sup>1</sup>, Efstratios Tzirtzilakis <sup>2,\*</sup>  and Mohammad Ferdows <sup>3</sup>

<sup>1</sup> Department of Mathematics, Comilla University, Cumilla 3506, Bangladesh; jahangircu1994@gmail.com (J.A.); limonn@yahoo.com (G.M.)

<sup>2</sup> Fluid Mechanics and Turbomachinery Laboratory, Department of Mechanical Engineering, University of the Peloponnese, 22100 Tripoli, Greece

<sup>3</sup> Research Group of Fluid Flow Modeling and Simulation, Department of Applied Mathematics, University of Dhaka, Dhaka 1000, Bangladesh; ferdows@du.ac.bd

\* Correspondence: etzirtzilakis@uop.gr

**Abstract:** In this study, we examined the biomagnetic flow and heat transfer of an incompressible electrically conductive fluid (blood) containing gold nanoparticles over a stretching sheet in the presence of a magnetic dipole. In this problem, both principles of magnetohydrodynamics (MHD) and ferrohydrodynamics (FHD) were adopted. Biot number and slip and suction parameters were taken into consideration. The nonlinear partial differential equations were transformed into ordinary differential equations by implementing similarity transformations. The numerical solution was attained by utilizing the *bvp4c* function technique in MATLAB R2018b software. The influence of pertinent parameters involved in this model, such as ferromagnetic parameter, magnetic field parameter, Grashof number, Eckert number, suction parameter, Biot number, slip parameter and Prandtl number, on the dimensionless velocity, temperature, skin friction and heat transfer rate were analyzed numerically and are represented graphically. Among the numerous results, it was observed that increment in ferromagnetic parameter and Prandtl number results in decrement of the velocity and temperature, respectively. For some values of the parameters, a comparison with the results of other documents in the literature is also made.

**Keywords:** nanofluid; thermophysical properties; gold nanoparticles; heat transfer; blood; BFD; MHD; FHD; stretching sheet



**Citation:** Alam, J.; Murtaza, G.; Tzirtzilakis, E.; Ferdows, M. Biomagnetic Fluid Flow and Heat Transfer Study of Blood with Gold Nanoparticles over a Stretching Sheet in the Presence of Magnetic Dipole. *Fluids* **2021**, *6*, 113. <https://doi.org/10.3390/fluids6030113>

Academic Editor: Ioannis Sarris

Received: 15 February 2021

Accepted: 2 March 2021

Published: 10 March 2021

**Publisher's Note:** MDPI stays neutral with regard to jurisdictional claims in published maps and institutional affiliations.



**Copyright:** © 2021 by the authors. Licensee MDPI, Basel, Switzerland. This article is an open access article distributed under the terms and conditions of the Creative Commons Attribution (CC BY) license (<https://creativecommons.org/licenses/by/4.0/>).

## 1. Introduction

Biomagnetic fluid is biological fluid that exists in living creatures under the influence of a magnetic field. Blood is one of the most common examples of a biomagnetic fluid. During the last few decades, studies on biomagnetic fluid have received more attention from researchers, due to its important applications in bioengineering and medical sciences, such as in magnetic device development for cell separation, reducing bleeding during surgeries and the targeted transport of drugs. Magnetic particles are also used for the magnetic resonance imaging (MRI) of specific ingredients of the human frame or cancer treatment [1–3].

In biomedical sciences, gold nanoparticles are the most important light-shedding material. Recently, the study of gold nanoparticles has gained serious attention from researchers due to gold nanoparticles' structure, shape, low toxicity and excellent compatibility with the human body.

In 1995, Choi [4] introduced a new fluid called nanofluid, in which nanoparticles are mixed with a base fluid such as blood, water or oil to improve their properties. In his study, he added small nanoparticles to a base fluid to increase the thermal conductivity.

The evaluation of gold nanoparticles started with the work of Faraday [5]. Akbari et al. [6] studied blood flow with gold nanoparticles (Au-NPs), where blood was treated as a third-grade non-Newtonian fluid. Numerical results were attained using Flex-PDE software, and the researchers found that the Grashof number is directly related to velocity profile. The effect of different shapes and structures of gold nanoparticles on cancer treatment and photo thermal therapy were examined by Huang et al. [7]. Olubode et al. [8] investigated the influence of partial slip and buoyancy on gold Carreau nanofluid flow, and they found that the fluid velocity is maximized when large values of partial slip and buoyancy are applied. The characteristics of blood with gold nanoparticles in the presence of thermal radiation in a porous channel with moving/stationary walls were numerically studied by Srinivas et al. [9]; they noticed that volume friction raises the temperature of the nanofluid. The impact of gold nanoparticles on Newtonian (water) and non-Newtonian (blood) fluid, considering the heat generation/absorption, was studied by Elgazery [10], who concluded that Au–blood heat transfer was comparatively higher than alumina–blood. The blade/spherical shape of Au-NPs in blood in exponential stretching sheets was considered and numerically studied by Eid [11]. An incompressible, electrically conductive nanofluid was investigated in the presence of a transverse magnetic field and a thermal radiation flux through an extending nanopolymer sheet by Ferdows et al. [12]. The principles of both magnetohydrodynamics (MHD) and ferrohydrodynamics (FHD) on BFD flow through a stenosis artery were examined by Jamal abadi et al. [13]. In their study, they found that wall temperature control can keep the blood in its ideal blood temperature range (below 40°C) and that a severe pressure drop occurs for blockages of more than 60 percent. Ferdows et al. [14] examined the simulation of blood flow and heat transfer through a stretching cylinder. Umair et al. [15] explored the study of MHD blood flow with Au-NPs considering radiation and transverse magnetic fields. They used the `bvp4c` function in MATLAB to calculate numerical results, and they found that the velocity of blood accelerates as the volume friction rises.

The aim of the present study was to investigate the biomagnetic flow and heat transfer of pure blood and gold pure blood under the effects of buoyancy, magnetic field, Biot number, suction, Navier slip and ferromagnetic number over a stretching sheet. The transformed similarity equations were solved numerically by using similarity transformations, and computational results were obtained with the help of the `bvp4c` function available in MATLAB software. Detailed discussion is presented regarding the variation of biomagnetic fluid velocity, temperature, skin friction and heat transfer rate. The validation of the numerical results presented was established by comparison with previously published results for some values of the parameters. We hope that the present study will be used in relevant biomedical and bioengineering studies.

## 2. Problem Formulation

In the presence of a magnetic dipole, an incompressible, electrically conductive biomagnetic fluid flow (namely blood) that contains gold nanoparticles (assumed to be of a spherical shape) and that passes through a two-dimensional stretched sheet was considered. Let the  $x$  axis be taken along the direction of the sheet and the  $y$  axis be normal. Consider that the fluid flow is from left to right, in the direction of the positive  $x$  axis. Moreover, assume that the temperature of the left-side sheet is  $T_f$ , while  $T_\infty$  is the right surface free stream temperature. A magnetic dipole creates a magnetic field of strength  $H$  under the sheet at distance  $d$  with magnetic field strength intensity  $B_0$  on the transverse direction on the plate. The geometry of the problem is depicted in Figure 1.

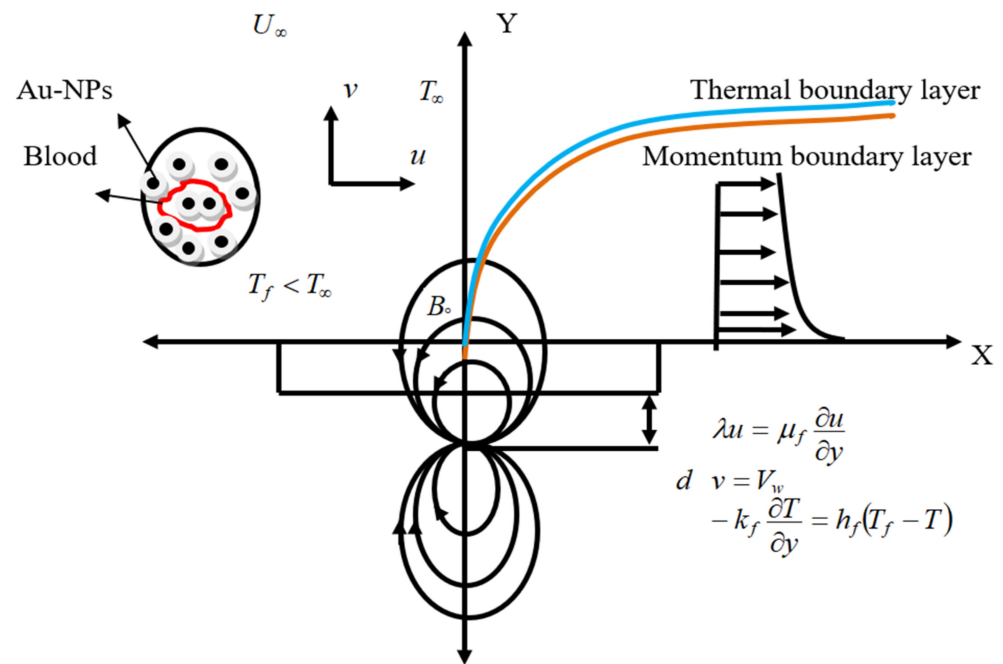


Figure 1. The geometry of the problem.

Under the assumptions of boundary layer approximations, as well as assumptions for the magnetic field, the governing equations for the problem conditions of both electrically conductivity and polarization can be written as [16]

$$\frac{\partial u}{\partial x} + \frac{\partial v}{\partial y} = 0 \tag{1}$$

$$u \frac{\partial u}{\partial x} + v \frac{\partial u}{\partial y} = U_\infty \frac{dU_\infty}{dx} + \frac{\mu_{nf}}{\rho_{nf}} \left( \frac{\partial^2 u}{\partial y^2} \right) + g\beta_{nf}(T - T_\infty) - \frac{\sigma_{nf} B_0^2 (u - U_\infty)}{\rho_{nf}} + \frac{\mu_0}{\rho_{nf}} M \frac{\partial H}{\partial x} \tag{2}$$

$$u \frac{\partial T}{\partial x} + v \frac{\partial T}{\partial y} + \frac{\mu_0}{(\rho C_p)_{nf}} T \frac{\partial M}{\partial T} \left( u \frac{\partial H}{\partial x} + v \frac{\partial H}{\partial y} \right) = \frac{K_{nf}}{(\rho C_p)_{nf}} \left( \frac{\partial^2 T}{\partial y^2} \right) + \frac{\mu_{nf}}{(\rho C_p)_{nf}} \left( \frac{\partial u}{\partial y} \right)^2 + \frac{\sigma_{nf} B_0^2 (u - U_\infty)^2}{(\rho C_p)_{nf}} \tag{3}$$

with appropriate boundary conditions:

$$\begin{aligned} \lambda u = \mu_f \frac{\partial u}{\partial y}, v = V_w, -k_f \frac{\partial T}{\partial y} = h_f [T_f - T] & \quad \text{at } y = 0 \\ u = U_\infty(x), T = T_\infty & \quad \text{as } y \rightarrow \infty \end{aligned} \tag{4}$$

where  $(u, v)$  represents the velocity components in the  $(x, y)$  direction.  $T$  is the nanofluid temperature;  $U_\infty(x) = ax$  is the free stream velocity;  $g$  represents the acceleration due to gravity;  $\lambda$  indicates slip coefficient;  $\mu, k, (\rho C_p), \beta, \rho, \sigma$  symbolize dynamic viscosity, thermal conductivity, heat capacity at constant pressure, the volumetric expansion coefficient, density and electrical conductivity and the subscript symbols  $nf, f, s$  indicate nanofluid, fluid and solid, respectively, which are defined as following form [16]

$$\begin{aligned} \mu_{nf} = \mu_f (1 - \phi)^{-2.5}, (\rho C_p)_{nf} = (1 - \phi)(\rho C_p)_f + \phi(\rho C_p)_s, \rho_{nf} = (1 - \phi)\rho_f + \phi\rho_s \\ \beta_{nf} = (1 - \phi)\beta_f + \phi\beta_s, \sigma_{nf} = (1 - \phi)\sigma_f + \phi\sigma_s, \frac{k_{nf}}{k_f} = \frac{(k_f + 2k_s) - 2\phi(k_f - k_s)}{(k_f + 2k_s) + \phi(k_f - k_s)} \end{aligned} \tag{5}$$

where  $\phi$  signifies volume fraction of nanoparticles ( $\phi = 0$  corresponding to a regular fluid).

The term  $\mu_0 M \frac{\partial H}{\partial x}$  denotes ferromagnetic body force per unit volume. This force will vanish in the absence of magnetic gradient [17]. The second term  $\mu_0 T \frac{\partial M}{\partial T} \left( u \frac{\partial H}{\partial x} + v \frac{\partial H}{\partial y} \right)$  in Equation (3) represents the heating due to adiabatic magnetization. Following [17], we assume that the horizontal and vertical magnetic field gradients are given by

$$\frac{\partial H}{\partial x} = \frac{\gamma}{2\pi} \frac{-2x}{(y+d)^4}, \frac{\partial H}{\partial y} = \frac{\gamma}{2\pi} \left[ \frac{-2}{(y+d)^3} + \frac{4x^2}{(y+d)^5} \right] \tag{6}$$

The force of the body is proportional to the gradient of magnitude  $H$ , which is

$$H(x, y) = [H_x^2 + H_y^2]^{\frac{1}{2}} = \frac{\gamma}{2\pi} \left[ \frac{1}{(y+d)^2} - \frac{x^2}{(y+d)^4} \right] \tag{7}$$

With the temperature  $T$  the impact of magnetization  $M$  is expressed as  $M = K(T - T_f)$ , where  $K$  is the pyromagnetic coefficient according to [18].

### 3. Solution Procedure

The governing equations were made dimensionless by introducing the following variables [16]

$$\eta = \sqrt{\frac{a}{\vartheta_f}} y, \psi = \sqrt{a\vartheta_f} x f(\eta), \theta(\eta) = \frac{T - T_\infty}{T_f - T_\infty} \tag{8}$$

The continuity equation is now satisfied as stream function  $\psi$  defined in the following form

$$u = \frac{\partial \psi}{\partial y} \text{ and } v = -\frac{\partial \psi}{\partial x} \tag{9}$$

After introducing Equation (9) into Equations (2)–(4), we obtain the following ordinary differential equations:

$$f'''' + (1 - \phi)^{2.5} (1 - \phi + \phi \frac{\rho_s}{\rho_f}) f f'' - (1 - \phi)^{2.5} (1 - \phi + \phi \frac{\rho_s}{\rho_f}) f'^2 + (1 - \phi)^{2.5} (1 - \phi + \phi \frac{\rho_s}{\rho_f}) + Gr (1 - \phi)^{2.5} (1 - \phi + \phi \frac{\rho_s}{\rho_f}) (1 - \phi + \phi \frac{\beta_s}{\beta_f}) \theta - (1 - \phi)^{2.5} (1 - \phi + \phi \frac{\sigma_s}{\sigma_f}) M (f' - 1) - (1 - \phi)^{2.5} \frac{2B\theta}{(\eta + \alpha)^3} = 0 \tag{10}$$

$$\theta'' + \frac{Pr k_f (1 - \phi + \phi \frac{\rho_s}{\rho_f})}{K_{nf}} f \theta' + \frac{Pr Eck_f}{K_{nf} (1 - \phi)^{2.5}} f'^2 + \frac{MPr Eck_f}{K_{nf}} (1 - \phi + \phi \frac{\sigma_s}{\sigma_f}) (f' - 1)^2 - \frac{2B\lambda_1 f (\epsilon + \theta) k_f}{K_{nf} (\eta + \alpha)^3} = 0 \tag{11}$$

The initial boundary conditions are:

$$f(0) = f_w, f'(0) = \beta f''(0), \theta'(0) = Bi[\theta(0) - 1], f'(\infty) = 1, \theta(\infty) = 0 \tag{12}$$

where,  $f_w$  is defined as the suction/injection parameter when  $f_w > 0$  and  $f_w < 0$ , representing suction and injection, respectively.

Here, Prandtl number  $Pr = \frac{(\mu c_p)_f}{k_f}$ , viscous dissipation parameter  $\lambda_1 = \frac{a\mu_f^2}{\rho_f \kappa_f (T_f - T_\infty)}$ , dimensionless Curie temperature  $\epsilon = \frac{T_\infty}{T_f - T_\infty}$ , the ferromagnetic interaction parameter  $B = \frac{\gamma}{2\pi} \frac{\mu_0 K (T_f - T_\infty) \rho_f}{\mu_f^2}$ , dimensionless distance  $\alpha = \sqrt{\frac{a}{\vartheta_f}} d$  from the origin to the center of the magnetic pole, Grashof number  $Gr = \frac{\beta_f g (T_f - T_\infty)}{U_\infty a}$ , the magnetic field parameter  $M = \frac{\sigma_f B_0^2}{\rho_f a}$ , the Eckert number  $Ec = \frac{U_\infty^2}{C_{pf} (T_f - T_\infty)}$ , slip parameter  $\beta = \frac{\mu_f}{\lambda} \sqrt{\frac{a}{\vartheta_f}}$  and the Biot number  $Bi = \frac{h_f}{k_f} \sqrt{\frac{\vartheta_f}{a}}$ .

The most interesting part of the study is the skin friction coefficient, the local Nusselt number, which is mathematically defined as

$$C_f = \frac{\tau_w}{\rho_f U_\infty^2} \tag{13}$$

$$Nu = \frac{xq_w}{k_f(T_f - T_\infty)} \tag{14}$$

where wall shear stress  $\tau_w$  and the heat flux  $q_w$  are given by

$$\tau_w = \mu_{nf} \left( \frac{\partial u}{\partial y} \right)_{y=0} \tag{15}$$

$$q_w = -k_{nf} \left( \frac{\partial T_1}{\partial y} \right)_{y=0} \tag{16}$$

With the help of similarity variables, the Equations (13) and (14) are reduced to

$$Re^{\frac{1}{2}} C_f = \frac{1}{(1-\phi)^{2.5}} f''(0) \text{ and } Re^{-\frac{1}{2}} Nu = -\frac{k_{nf}}{k_f} \theta'(0) \tag{17}$$

#### 4. Numerical Method for Solution

In order to solve Equations (10) and (11) subject to the boundary condition (12), we reformed the boundary value problem to be in a compatible form for the solver (bvp4c) function in MATLAB software. For this we needed to convert Equations (10) and (11) along with Equation (12) into first order differential equations by assuming new variables. We estimated the initial variable in the following way:  $f = y_1, f' = y_2, f'' = y_3, \theta = y_4, \theta' = y_5$ . Then, the equations and boundary conditions were transformed into a system of first order ordinary differential equations as given below.

$$\begin{aligned} f' &= y_2, f'' = y_2' = y_3 \\ f''' = y_3' &= -(1-\phi)^{2.5} \left( 1 - \phi + \phi \frac{\rho_s}{\rho_f} \right) y_1 y_3 + (1-\phi)^{2.5} \left( 1 - \phi + \phi \frac{\rho_s}{\rho_f} \right) y_2^2 - (1-\phi)^{2.5} \left( 1 - \phi + \phi \frac{\rho_s}{\rho_f} \right) \\ &- (1-\phi)^{2.5} \left( 1 - \phi + \phi \frac{\rho_s}{\rho_f} \right) \left( 1 - \phi + \phi \frac{\beta_s}{\beta_f} \right) Gr y_4 + (1-\phi)^{2.5} \left( 1 - \phi + \phi \frac{\sigma_s}{\sigma_f} \right) M (y_2 - 1) + (1-\phi)^{2.5} \frac{2B y_1}{(\eta+\alpha)^4} \\ \theta' &= y_5 \\ \theta'' = y_5' &= -\frac{k_f}{k_{nf}} PrEc \left[ (1-\phi) + \phi \frac{(\rho c_p)_s}{(\rho c_p)_f} \right] y_1 y_5 - \frac{k_f}{k_{nf}} \frac{PrEc}{(1-\phi)^{2.5}} y_3^2 \\ &- \frac{k_f}{k_{nf}} PrEc M \left( 1 - \phi + \phi \frac{\sigma_s}{\sigma_f} \right) (y_2 - 1)^2 + \frac{k_f}{k_{nf}} \frac{2B \lambda_1 y_1 (\epsilon + \theta)}{(\eta + \alpha)^3} \end{aligned} \tag{18}$$

subject to the boundary conditions:

$$y_2(0) = \beta y_3(0), y_1(0) = f_w, y_4(0) = Bi[y_1(0) - 1], y_2(\infty) = 1, y_4(\infty) = 0 \tag{19}$$

Equations (18) and (19) are integrated numerically as an initial value problem to a given terminal point. All these simplifications were made by using the bvp4c function available in MATLAB software.

#### 5. Comparison with Previous Work and Values of Thermophysical Properties

The values of thermophysical properties of blood are given in Table 1. It is noted that the thermophysical properties of gold are widely known and easy to find in general property tables. For blood, on the contrary, the properties are not so easy to find, and it was noticed that tables with mistakes have been published. For the properties of blood presented in Table 1, we considered the verified values referenced or calculated from the following studies [19–24].

**Table 1.** Thermophysical properties of blood and gold nanoparticles (spherical shape).

Thermo Physical Properties	Blood	Gold
$C_p(J/kgK)$	$3.9 \times 10^3$	129
$\rho(Kg/m^3)$	1050	19,300
$\sigma(S/m)$	0.8	$4.1 \times 10^{-7}$
$k(W/mK)$	0.5	318
$\beta(1/K)$	$4 \times 10^{-4}$	$1.4 \times 10^{-5}$

To ensure the accuracy and validity of our study, we compared the present numerical Nusselt number values with those of Daniel’s [19] various values of non-linear stretching parameter  $n$  and Prandtl number  $Pr$  for  $B = \phi = Gr = Ec = 0, k_{nf} = k_f = 1$ . The comparison shows an excellent agreement as presented in Table 2. To further ensure the numerical code validation, we conducted a numerical comparison with the study of [16], as clearly depicted in Figures 2 and 3, and this further confirmed the suitability of this numerical code for this model.

**Table 2.** Comparison for values of  $-\theta'(0)$  between different values of  $n$  and  $Pr$ .

Pr	$n$	Daniel [19]	Present Result	error %
1	0.2	0.610262	0.610112	0.0246
1	0.5	0.595277	0.595863	0.0984
1	1.5	0.574537	0.574898	0.0629
5	0.2	0.607175	0.607160	0.0024
5	0.5	1.586744	1.607160	1.2869
5	1.5	1.557413	1.557214	0.0128

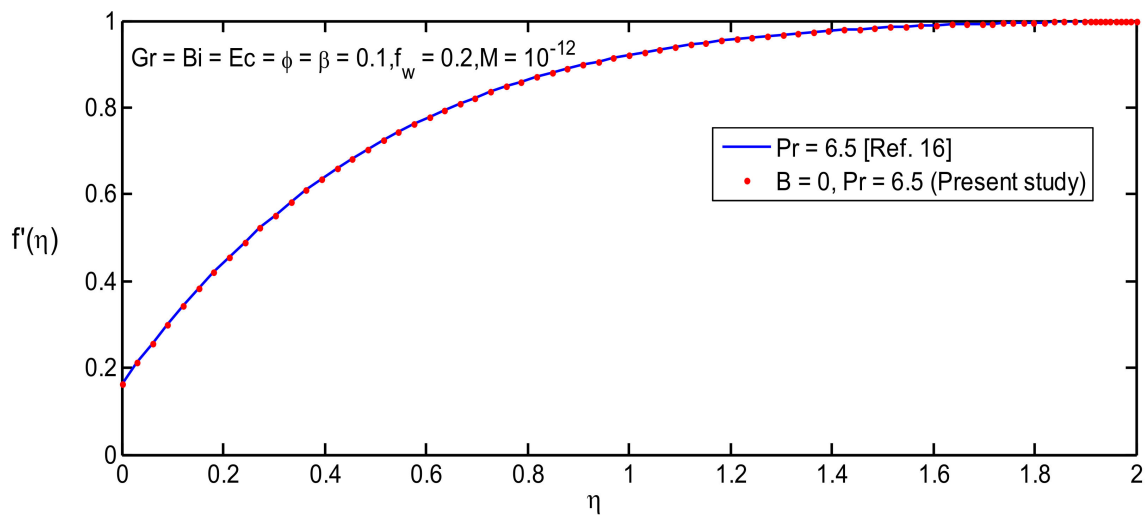


**Figure 2.** Comparison of velocity profile for  $B = 0$ .

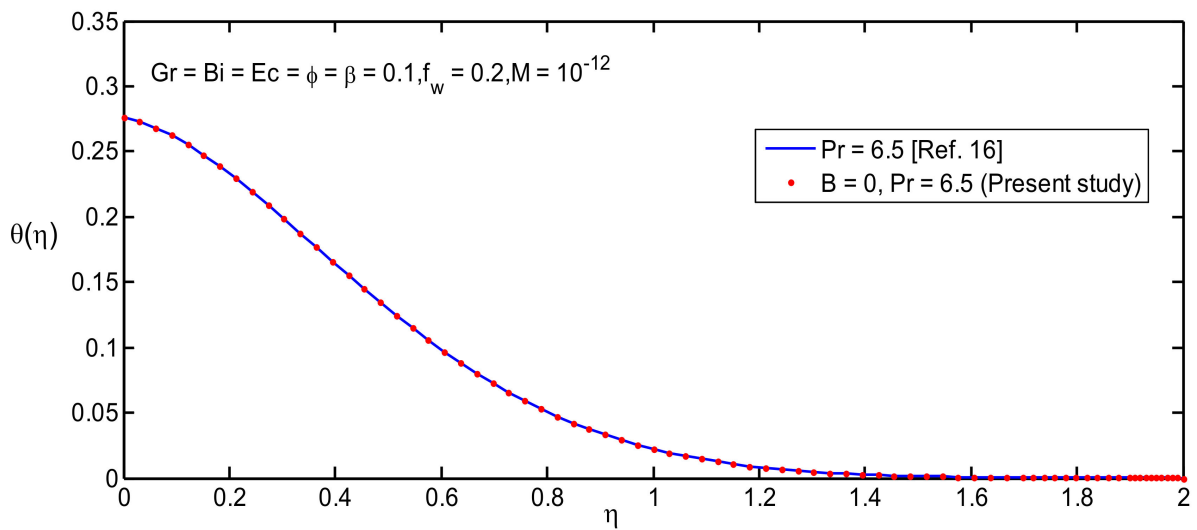


Figure 3. Comparison of Temperature profile for  $B = 0$ .

### 6. Results and Discussion

The results of the numerical calculations for the solution of the system (18) subject to the boundary conditions (19) are placed in this section.

When assigning values to the numerous parameters for the problem under consideration, we adopted values published in previous studies as follows: Prandtl number  $Pr = 17, 21, 25$  as in [22], and ferromagnetic number  $B = 0$  to 10 as in [14,22]—note that  $B = 0$  corresponds to hydrodynamic flow; volume friction  $\phi = 0.0, 0.001, 0.002, 0.02, 0.1$  as in [16]; dimensionless distance  $\alpha = 1.0$  as in [22]; magnetic field parameter  $M = 1, 2, 3$  as in [24]; Grashof number  $Gr = 1, 2, 3$  as in [16]; Eckert number  $Ec = 1, 2, 3$  as in [16]; suction parameter  $f_w = 0.5, 1.0, 1.5$  as in [16]; velocity slip parameter  $\beta = 0.5, 1.0, 1.5$  as in [16]; Biot number  $Bi = 0.1, 0.3, 0.5, 0.7$  as in [16] and temperature of the Curie number  $\varepsilon = 78.5$  and the viscous dissipation number  $\lambda_1 = 6.4 \times 10^{-14}$  [25,26].

Figures 4 and 5 depict the velocity and temperature profiles for various values of suction parameter ( $f_w$ ). From the figures it is observed that the velocity profile increases and temperature profiles decrease with increasing values of suction parameter in both cases for pure blood and gold pure blood.

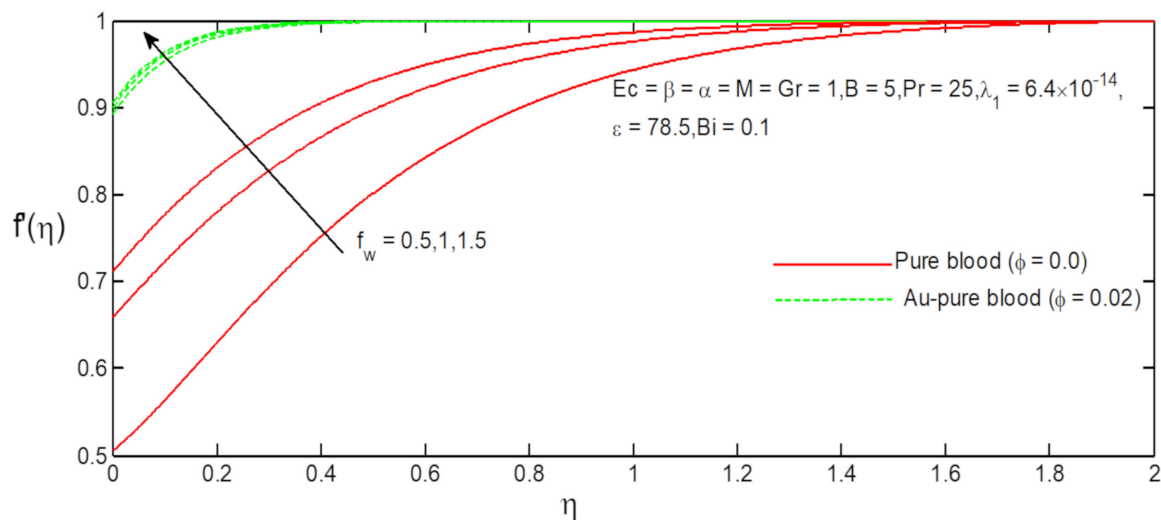


Figure 4. Influence of  $f_w$  on  $f'(\eta)$ .

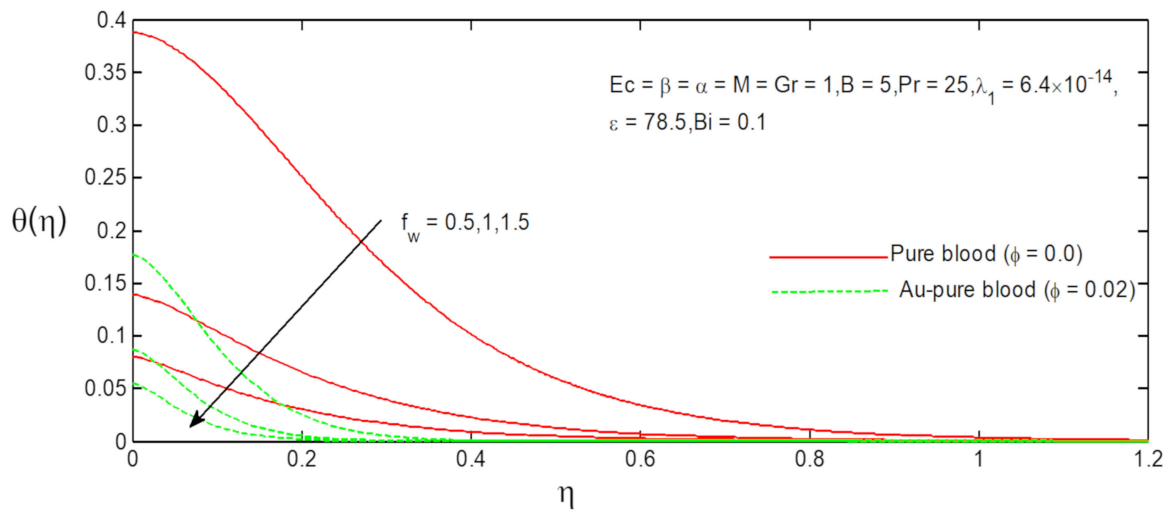


Figure 5. Influence of  $f_w$  on  $\theta(\eta)$ .

Figures 6 and 7 depict the velocity and temperature profiles for various values of velocity slip parameter ( $\beta$ ). From the figures it is observed that velocity profile increases and temperature profiles decrease with increasing values of slip parameter in both cases for pure blood and gold pure blood.

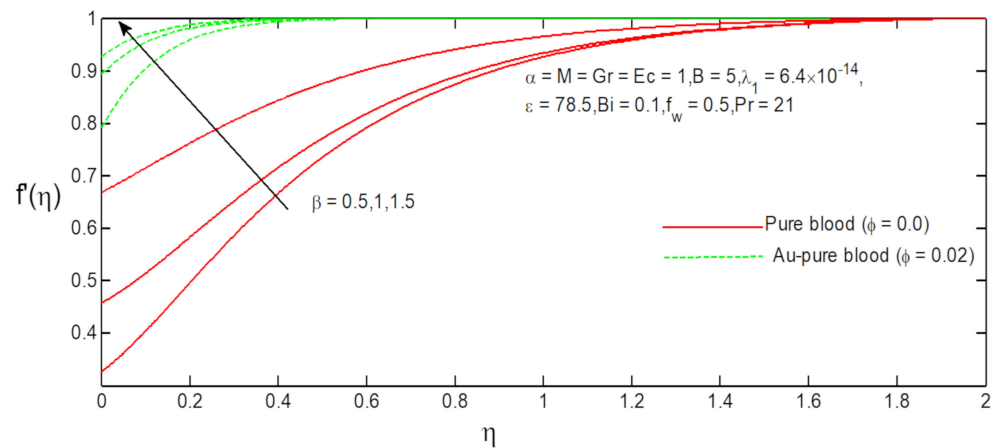


Figure 6. Influence of  $\beta$  on  $f'(\eta)$ .

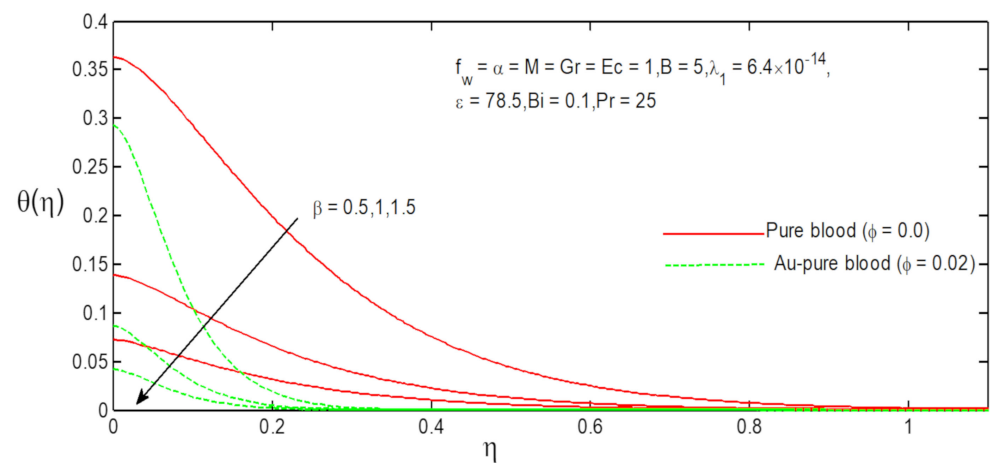


Figure 7. Influence of  $\beta$  on  $\theta(\eta)$ .

The effect of Biot number ( $Bi$ ) on velocity and temperature distribution can be found in Figures 8 and 9. From the figures it is observed that velocity profile increases with increasing values of Biot number in the case of pure blood but decreases for gold pure blood. On the other hand, temperature profiles increase with increasing values of Biot number. This increment can be justified due to the fact that increment of convective heat exchange at the sheet results in an increase in thermal boundary layer thickness.

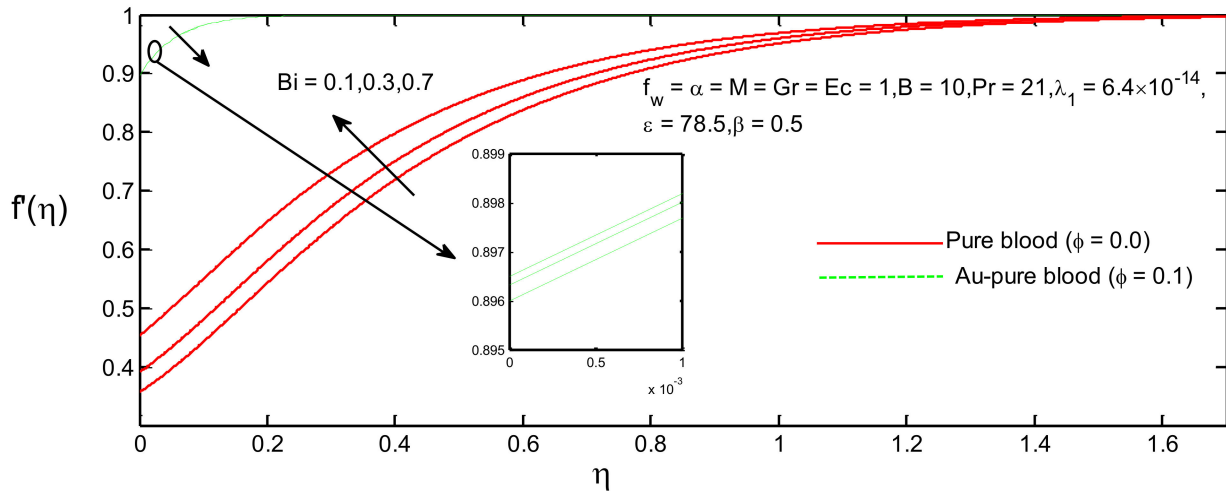


Figure 8. Influence of  $Bi$  on  $f'(\eta)$ .

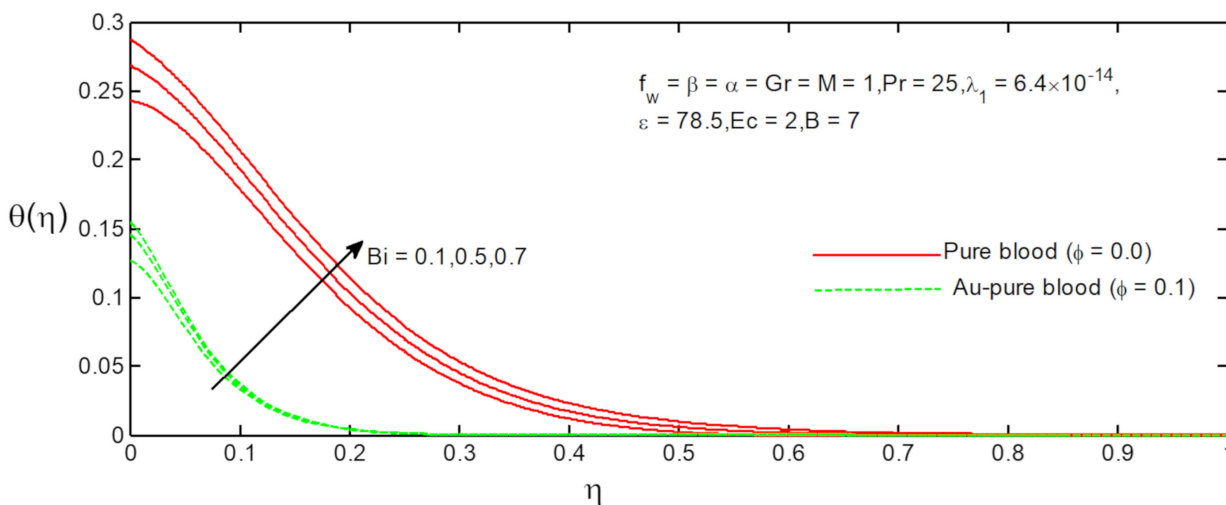


Figure 9. Influence of  $Bi$  on  $\theta(\eta)$ .

The velocity and temperature distributions for different values of the ferromagnetic number ( $\beta$ ) are represented in Figures 10 and 11. From the figures it can be clearly observed that temperature profile increases and velocity profile decreases due to the presence of ferrite nanoparticles as the ferromagnetic number values increase.

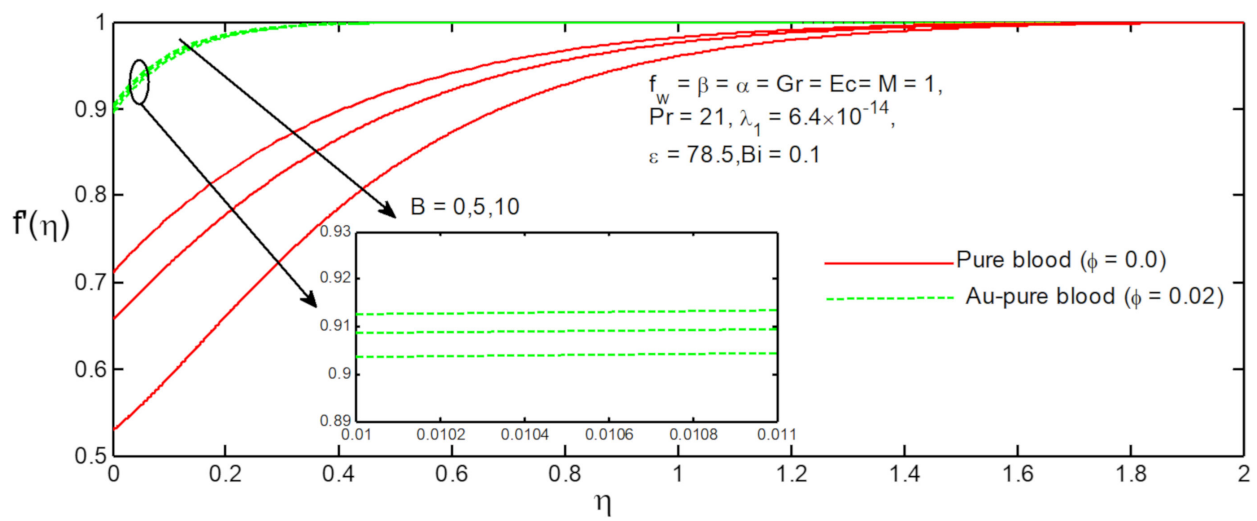


Figure 10. Influence of  $B$  on  $f'(\eta)$ .

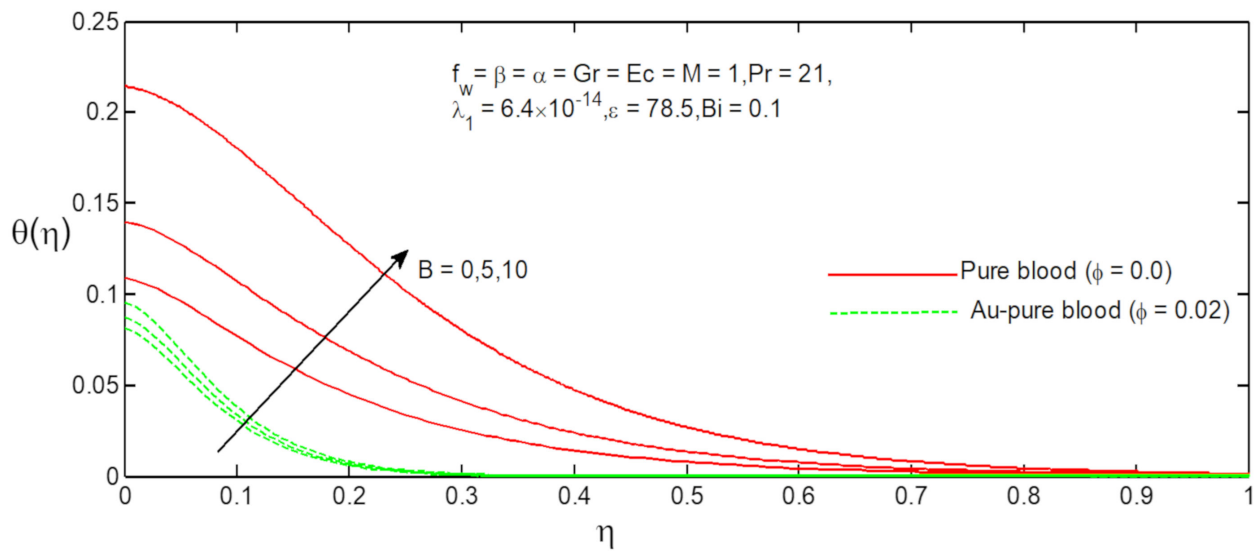


Figure 11. Influence of  $B$  on  $\theta(\eta)$ .

Figures 12 and 13 present the effect of Grashof number ( $Gr$ ) on distributions of velocity and temperature. It can be noted that fluid velocity increases and temperature decreases because the Grashof number is the ratio of thermal buoyancy force to hydrodynamic force.

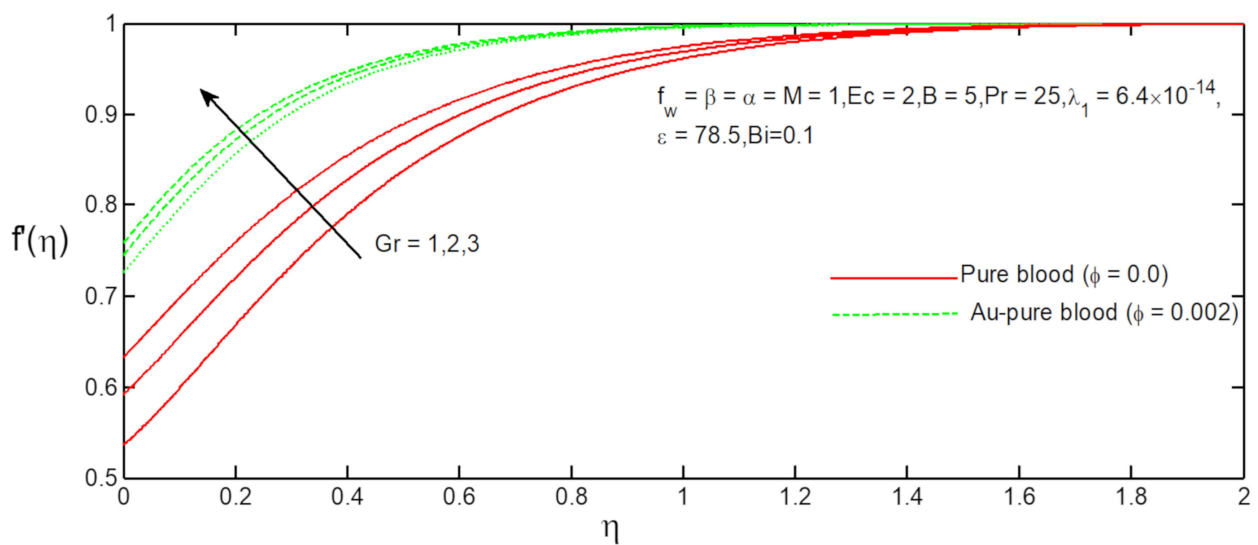


Figure 12. Influence of  $Gr$  on  $f'(\eta)$ .

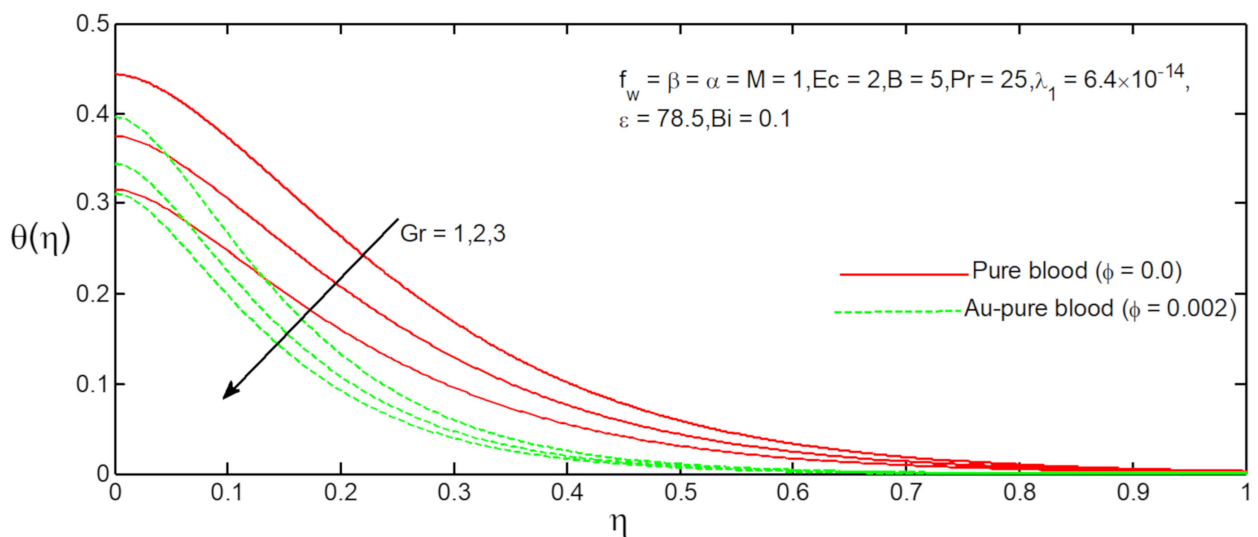


Figure 13. Influence of  $Gr$  on  $\theta(\eta)$ .

Figures 14 and 15 depict the velocity and temperature profiles for various values of the Eckert number ( $Ec$ ). It was found that velocity profile increase with increasing values of the Eckert number in the case of pure blood but decreases for the case of gold particles and blood. Temperature profiles increase with increasing values of Eckert number, and this could be explained by the heat addition caused by frictional heating.

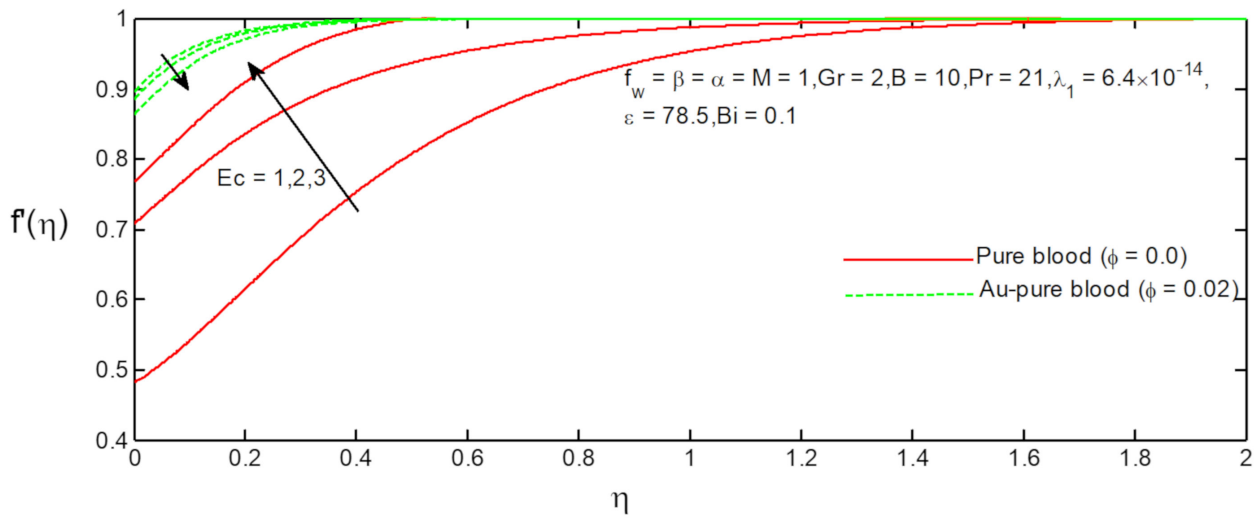


Figure 14. Influence of  $Ec$  on  $f'(\eta)$ .

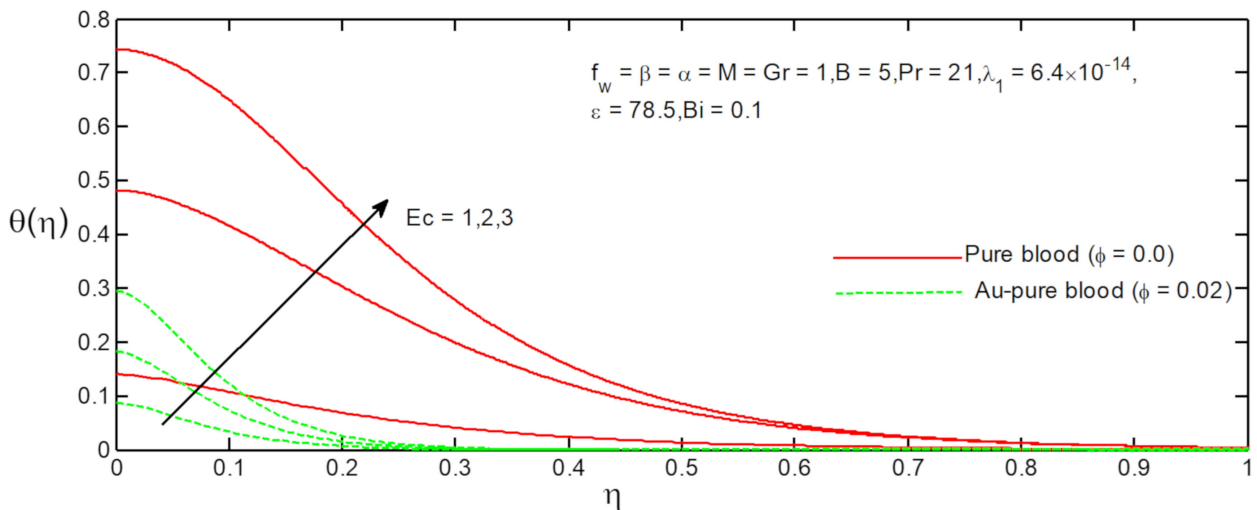


Figure 15. Influence of  $Ec$  on  $\theta(\eta)$ .

Figures 16 and 17 depict the velocity and temperature profiles for various values of magnetic field parameter ( $M$ ). From Figure 17 it is observed that temperature profiles decrease with increasing values of magnetic field parameter in both cases for pure blood and gold pure blood. From Figure 16, it is observed that the velocity boundary layer thickness is increased as the magnetic parameter increases. This is because the presence of the transverse magnetic field causes the appearance of the Lorentz force in the electrically conductive fluid.

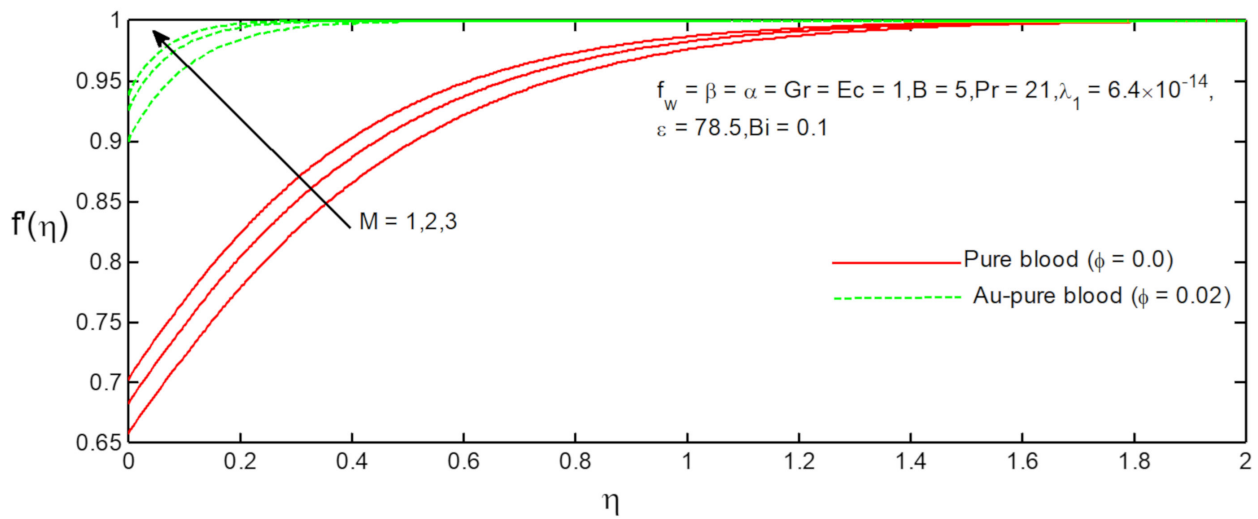


Figure 16. Influence of  $M$  on  $f'(\eta)$ .

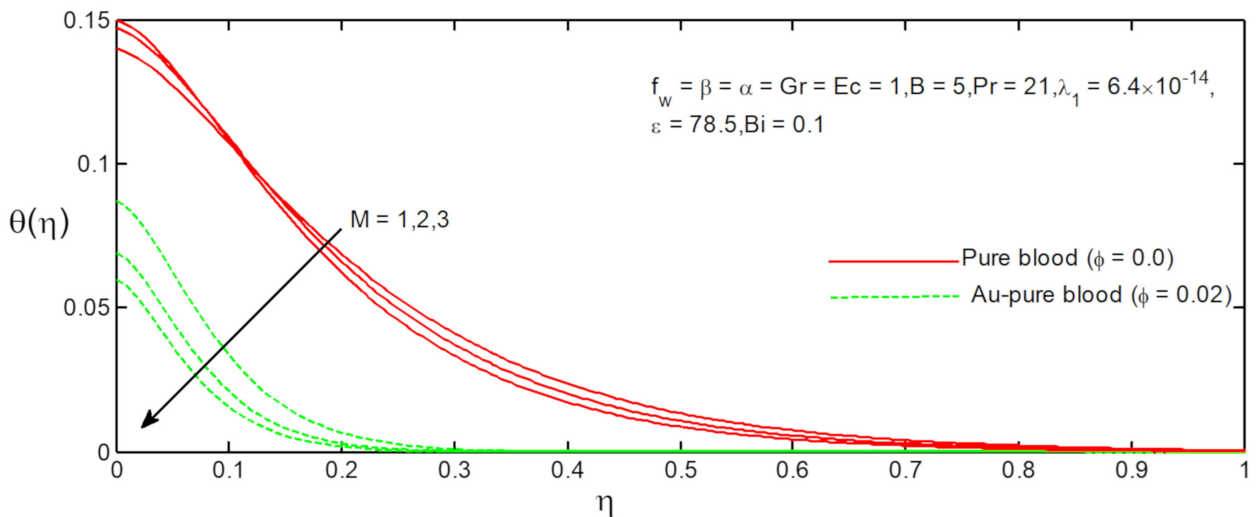


Figure 17. Influence of  $M$  on  $\theta(\eta)$ .

The influence of Prandtl number ( $Pr$ ) on dimensionless velocity and temperature profile is illustrated in Figures 18 and 19. From the figures it is observed that velocity profile increases and temperature profile decreases with increasing values of the Prandtl number. Clearly, the Prandtl number expresses the ratio of the momentum diffusion to thermal diffusion. In other words, the Prandtl number is the ratio of the kinematic viscosity of the fluid to its thermal diffusivity. This means that a higher Prandtl number results in lower thermal conductivity, and this is why increasing Prandtl number values have the effect of decreased temperature profiles.

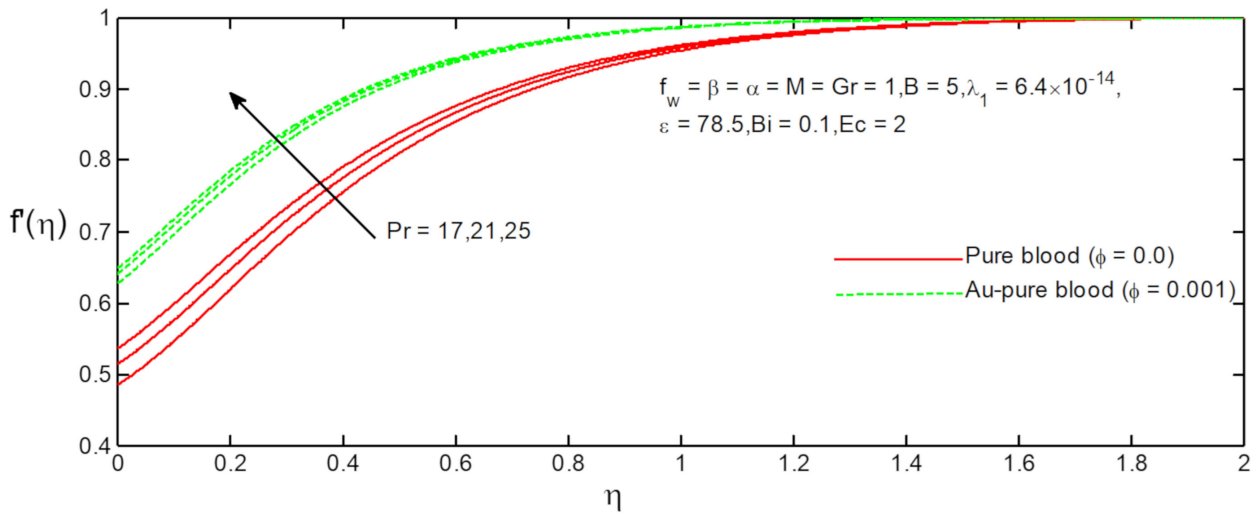


Figure 18. Influence of Pr on  $f'(\eta)$ .

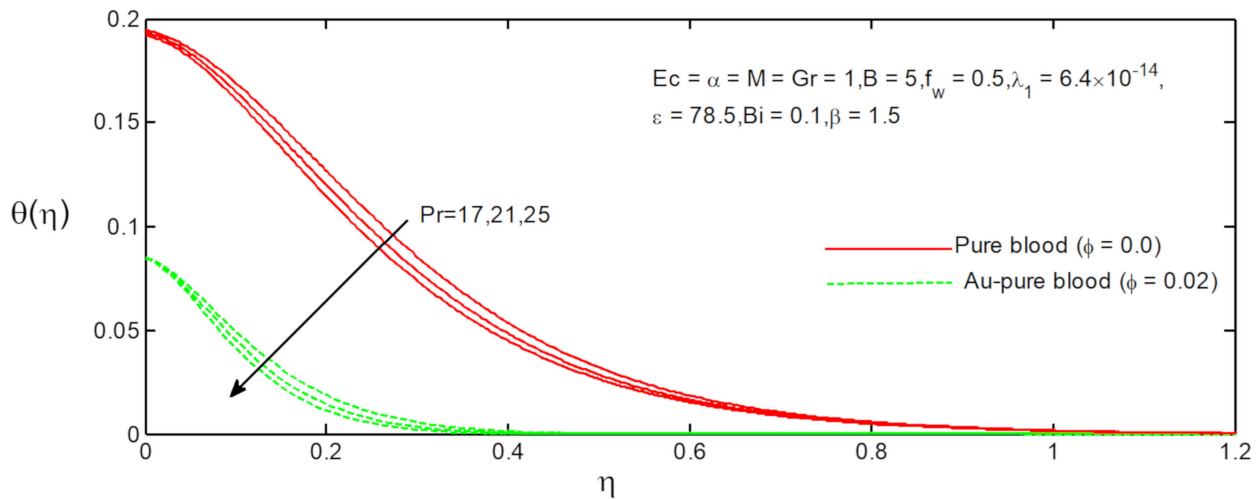


Figure 19. Influence of Pr on  $\theta(\eta)$ .

Figures 20–25 demonstrate the skin friction coefficient and heat transfer rate for various values of Eckert number, ferromagnetic number, Grashof number, suction parameter, Prandtl number and slip parameter with respect to the magnetic field parameter. From Figures 20 and 21, it is observed that  $-\theta'(0)$  increases with Eckert and ferromagnetic numbers, whereas  $-\theta'(0)$  decreases with Grashof number and suction parameter (see Figures 22 and 23). From Figures 24 and 25, it is observed that  $f''(0)$  decreases as Prandtl number and slip parameter increase.

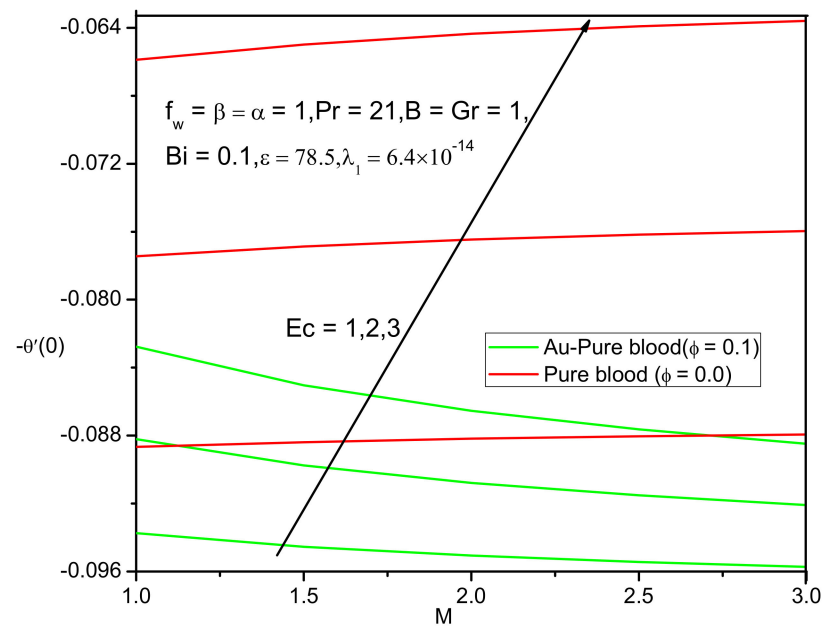


Figure 20. Local Nusselt number  $-\theta'(0)$  with  $M$  for different values of  $Ec$ .

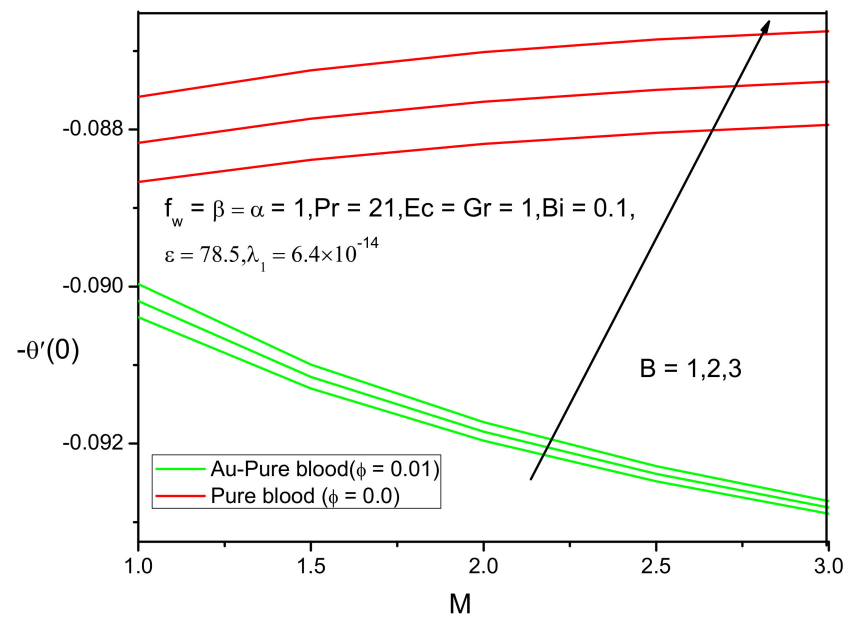


Figure 21. Local Nusselt number  $-\theta'(0)$  with  $M$  for different values of  $B$ .

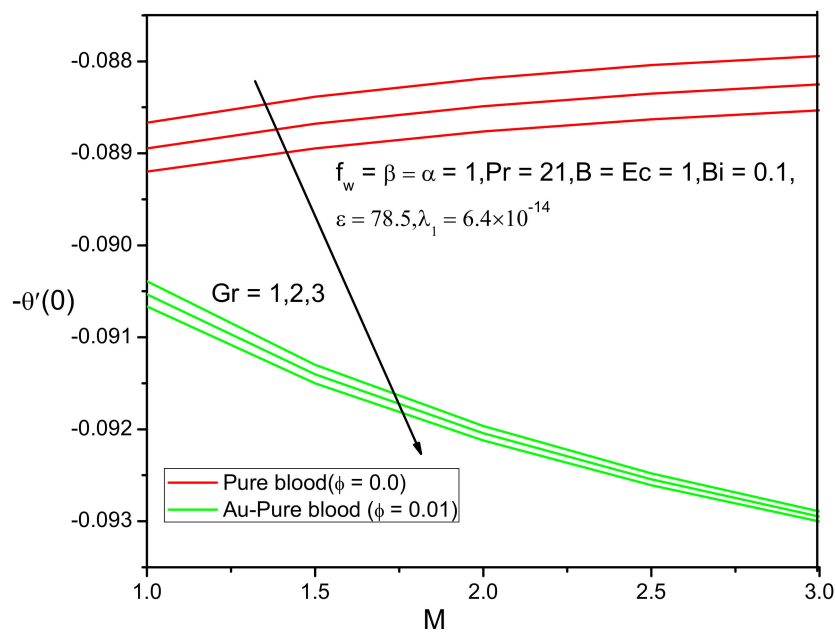


Figure 22. Local Nusselt number  $-\theta'(0)$  with  $M$  for different values of  $Gr$ .

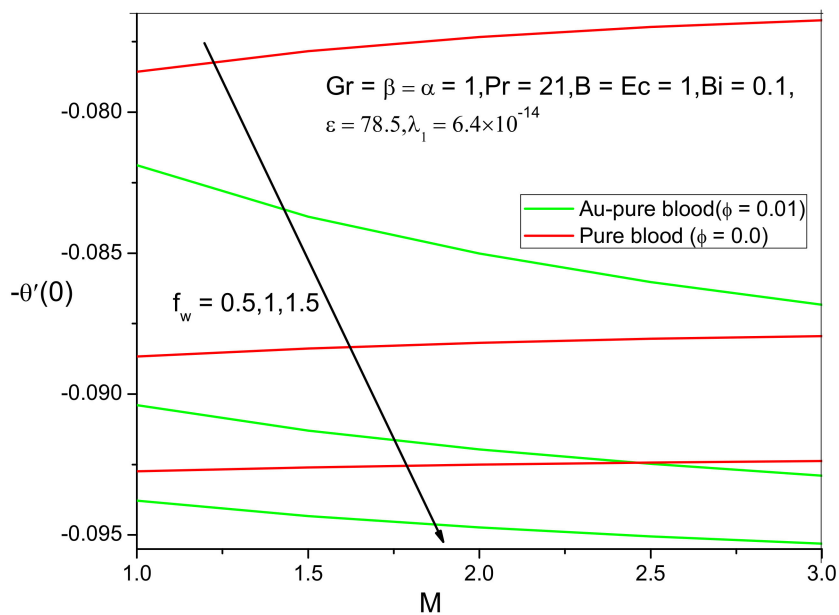


Figure 23. Local Nusselt number  $-\theta'(0)$  with  $M$  for different values of  $f_w$ .

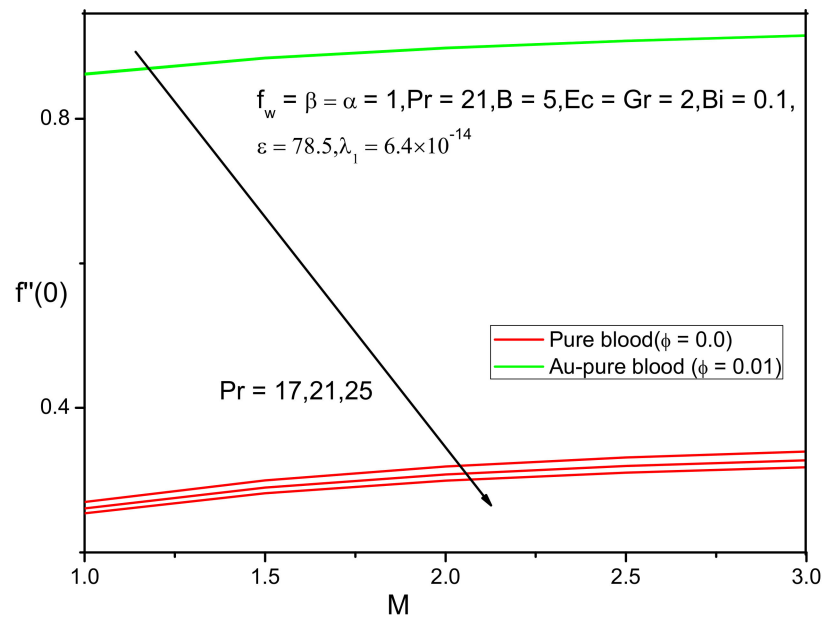


Figure 24. Skin friction coefficient  $f''(0)$  with  $M$  for different values of  $Pr$ .

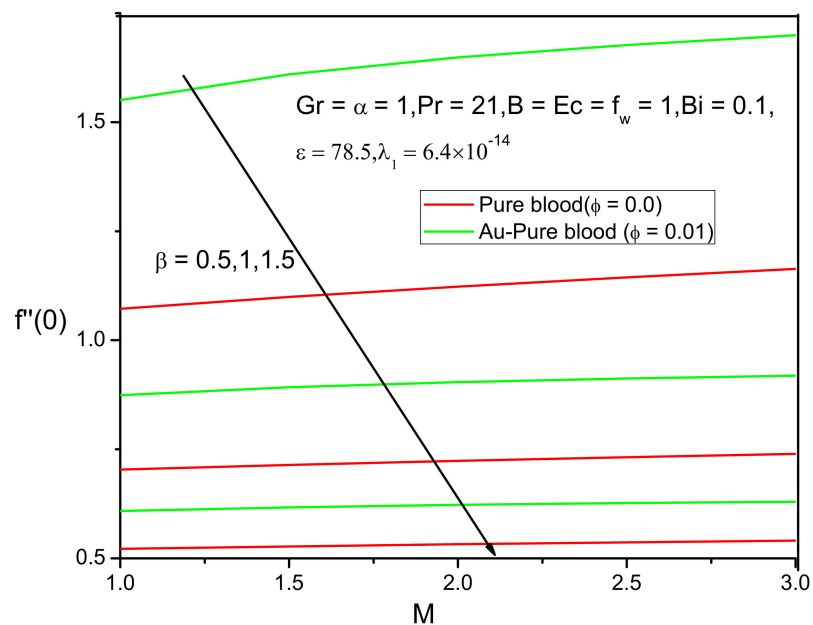


Figure 25. Skin friction coefficient  $f''(0)$  with  $M$  for different values of  $\beta$ .

### 7. Conclusions

In the present study, we studied the biomagnetic flow and heat transfer of incompressible, electrically conductive blood containing gold (Au) nanoparticles flowing over a stretching sheet in the presence of a magnetic dipole. The major conclusions of this work are as follows:

- The velocity profiles of Au-pure blood and pure blood nanofluid increase with increasing values of suction parameter, slip parameter, Grashof number, magnetic field parameter and Prandtl number;
- The temperature profiles of Au-pure blood and pure blood nanofluid increase with increasing values of Ferromagnetic field parameter;
- The velocity profiles of pure blood nanofluid increase with increasing values of Biot number and Eckert number, whereas those of Au-pure blood decrease in these cases;

- The skin friction coefficient of Au-pure blood and pure blood nanofluid decreases with increased values of Prandtl number and slip parameter;
- The heat transfer rate of Au-pure blood and pure blood nanofluid is augmented with increasing values of Eckert number and ferromagnetic parameter;
- The heat transfer rate of Au-pure blood and pure blood nanofluid decreases with increasing values of Grashof number and suction parameter.

**Author Contributions:** Conceptualization, M.F. and G.M.; methodology, G.M. and M.F.; software, J.A. and G.M.; validation, E.T., M.F. and G.M.; formal analysis, J.A.; investigation, J.A. and G.M.; resources, M.F.; data curation, J.A. and M.F.; writing—original draft preparation, J.A. and G.M.; writing—review and editing, E.T.; visualization, J.A.; supervision, G.M. and E.T.; project administration, M.F.; funding acquisition, G.M. All authors have read and agreed to the published version of the manuscript.

**Funding:** This research received no external funding.

**Institutional Review Board Statement:** Not applicable.

**Informed Consent Statement:** Not applicable.

**Data Availability Statement:** Not applicable.

**Conflicts of Interest:** The authors declare no conflict of interest.

## References

1. Misra, J.C.; Sinha, A.; Shit, G.C. Flow of a biomagnetic viscoelastic fluid: Application to estimate of blood flow in arteries during electromagnetic hyperthermia, a therapeutic procedure for cancer treatment. *App. Math. Mech. Engl.* **2010**, *31*, 1405–1420. [[CrossRef](#)]
2. Nelson, P.W.; Gilchrist, M.A.; Coombs, D.; Hyman, J.M.; Perelson, A.S. An age-structured model of HIV infection that allow for variations in the production rate of viral particles and the death rate of productively infected cells. *Math. Biosci. Eng.* **2004**, *1*, 267–288. [[CrossRef](#)]
3. Wang, J.; Dong, X. Analysis of an HIV infection model incorporating latency age and infection age. *Math. Biosci. Eng.* **2018**, *15*, 569–594. [[CrossRef](#)]
4. Choi, S.U.S. Enhancing thermal conductivity of fluids with nanoparticles. In Proceedings of the ASME International Mechanical Engineering Congress and Exposition, San Francisco, CA, USA, 12–18 November 1995; pp. 99–105.
5. Michael, Faraday's Gold Colloids, The Royal Institution: Science Lives Here. Available online: [www.rigb.org](http://www.rigb.org) (accessed on 4 December 2015).
6. Akbari, N.; Ganji, D.D.; Gholinia, M.; Gholinia, S. Computer simulation of blood flow with nanoparticles in a magnetic field as a third grade non-Newtonian through porous vessels by flex PDE software. *Innov. Ener. Res.* **2017**, *6*, 1–7.
7. Huang, X.; El-Sayed, M.A. Gold nanoparticles and implementations in cancer diagnosis and photo thermal therapy. *J. Adv. Res.* **2010**, *1*, 13–28. [[CrossRef](#)]
8. Olubode, K.K.; Issac, L.C.; Mahanthesh, B.; Salman, S. Heat transfer in the flow of Blood-gold carreaunanofluid induced by partial slip and buoyancy. *Heat Transf. Asia Res.* **2018**, *47*, 806–823. [[CrossRef](#)]
9. Srinivas, S.; Vijayalakshmi, A.; Reddy, A.S. Flow and heat transfer of gold-blood nanofluid in a porous channel with moving/stationary walls. *J. Mech.* **2017**, *33*, 395–404. [[CrossRef](#)]
10. Elgazery, N.S. Flow of non-Newtonian magneto fluid with gold and alumina nanoparticles through a non Darcian porous medium. *J. Egypt. Math. Soc.* **2019**, *27*. [[CrossRef](#)]
11. Eid, M.R. Effects of nanoparticles shapes on non-Newtonian Bio-nanofluid flow in a suction/Blowing process with convective condition: Sisko model. *J. Non Equilib. Thermodyn.* **2019**, *45*. [[CrossRef](#)]
12. Ferdows, M.; Khan, M.S.; Bég, O.A.; Azad, M.A.K.; Alam, M.M. Numerical study of transient magnetohydrodynamic radiative free convection nanofluid flow from a stretching permeable surface. *J. Process. Mech. Eng.* **2014**, *228*, 181–196. [[CrossRef](#)]
13. Jamal abadi, M.Y.A.; DaqiqShirazi, M.; Nasiri, H.; Safaei, M.R.; Nguyen, T.K. Modeling and analysis of biomagnetic blood Carreau fluid flow through a stenosis artery with magnetic heat transfer: A transient study. *PLoS ONE* **2018**, *13*, e0192138.
14. Ferdows, M.; Murtaza, M.G.; Tzirtzilakis, E.E.; Alzahrani, F. Numerical study of blood flow and heat transfer through stretching cylinder in the presence of a magnetic dipole. *Z. Angew. Math. Mech.* **2020**, *100*, e201900278. [[CrossRef](#)]
15. Umair, K.; Anum, S.; Aurang, Z.; El-Sayed, M.S.; Dumitru, B. MHD radiative blood flow embracing gold particles via a slippery sheet through an erratic heat source/sink. *Mathematics* **2020**, *8*, 1597. [[CrossRef](#)]
16. Mutuku-Njane, W.N.; Makinde, O.D. Combined effect of buoyancy force and Navier slip on MHD flow of a Nanofluid over a convectively heated vertical porous plate. *Sci. World J.* **2013**. [[CrossRef](#)]
17. Tzirtzilakis, E.E. A simple numerical methodology for BFD problems using stream function vortices formulation. *Commun. Numer. Methods Eng.* **2000**, *2*, 1–6.

18. Anderson, H.I.; Valens, O.A. Flow of a heated Ferro fluid over a stretching sheet in the presence of a magnetic dipole. *Acta Mech.* **1998**, *28*, 39–47. [[CrossRef](#)]
19. Daniel, Y.S. Steady MHD boundary-layer slip flow and heat transfer of Nanofluid over a convectively heated of a non-linear permeable sheet. *J. Adv. Mech. Eng.* **2016**, *3*, 1–14. [[CrossRef](#)]
20. Tzirtzilakis, E.E. A mathematical model for blood flow in magnetic field. *Phys. Fluids* **2005**, *17*, 077103. [[CrossRef](#)]
21. Gabriely, S.; Lau, R.W.; Gabriel, C. The dielectric properties of biological tissues: III. Parametric models for the dielectric spectrum of tissues. *Phys. Med. Biol.* **1996**, *41*, 2271–2293. [[CrossRef](#)]
22. Hinghofer-Szalkay, H. Volume and density changes of biological fluids with temperature. *J. Appl. Physiol.* **1985**, *59*, 1686–1689. [[CrossRef](#)]
23. Tzirtzilakis, E.E. Biomagnetic fluid flow in an aneurysm using ferrohydrodynamics principles. *Phys. Fluids* **2015**, *27*, 061902. [[CrossRef](#)]
24. Reddy, S.R.R.; Reddy, P.B.A. Biomathematical analysis for the stagnation point flow over a nonlinear stretching surface with the second order velocity slip and Titanium alloy nanoparticle. *Front. Heat Mass Transf.* **2018**, *10*. [[CrossRef](#)]
25. Alam, M.J.; Murtaza, M.G. Two Dimensional Biomagnetic fluid flow and heat transfer over a nonlinear stretching sheet with temperature dependent viscosity. *Sch. J. Phys. Math. Stat.* **2020**, *7*, 131–142. [[CrossRef](#)]
26. Murtaza, M.G.; Ferdows, M.; Misra, J.C.; Tzirtzilakis, E.E. Three-dimensional biomagnetic Maxwell fluid flow over a stretching surface in presence of heat source/sink. *Int. J. Biomath.* **2019**, *12*, 1950036–20. [[CrossRef](#)]